Composite Structures 223 (2019) 110956

Contents lists available at ScienceDirect

Composite Structures

journal homepage: www.elsevier.com/locate/compstruct

Measured dynamic properties for FRP footbridges and their critical comparison against structures made of conventional construction materials

Xiaojun Wei[a,b,*], Justin Russell[b], Stana Živanović[c], J. Toby Mottram[b]

[a] School of Civil Engineering, Central South University, Changsha 410075, China
[b] School of Engineering, University of Warwick, Coventry CV4 7AL, UK
[c] College of Engineering, Mathematics and Physical Sciences, University of Exeter, Exeter EX4 4QF, UK

ARTICLE INFO

Keywords:
FRP composite
Footbridge
Modal property
Amplitude dependence
Resonance response

ABSTRACT

This paper reports new experimental data for dynamic properties (i.e. modal mass, natural frequency and damping ratio) of eight FRP composite footbridges in Europe, which helps to resolve the weakness in knowledge and understanding of dynamic properties of FRP footbridges. In addition, dynamic properties are reviewed with the results of six other FRP footbridges and 124 non-FRP footbridges built after 1991. A comprehensive comparison of these 138 sets of dynamic properties shows that FRP footbridges possess similar fundamental frequencies at the same span, but usually higher damping ratios (mean of 2.5% c.f. mean of < 1.0% for steel, concrete and steel-concrete composite). Additionally, natural frequencies and damping ratios identified from free decays measured on FRP footbridges are response amplitude dependent. Comparing the accelerance peaks of FRP and conventional footbridges revealed that the FRP footbridges are, on average, around 3.5 times more responsive to resonant excitation than the conventional bridges having the same bridge length, deck width and mode shape due to their significantly lower modal mass.

1. Introduction

Fibre-reinforced polymer (FRP) composite shapes and systems are increasingly used in the construction sector, motivated by their successful structural applications in aviation, chemical, offshore oil and gas, rail and marine sectors. Advantages of FRPs over other construction materials in structures, such as footbridges, are their high strength- and stiffness-to-weight ratios, low maintenance costs and quick installations. In the last four decades, hundreds of FRP bridges, typically short (i.e. spans less than 20 m) to medium span (i.e. spans ranging from 20 m to 80 m), have been built around the world [1,2]. A reason for hesitation in constructing longer span bridges can be the excessive vibration that FRP bridges, featured by lightweight and liveliness, might potentially possess under serviceability actions [3,4], causing user discomfort. Vibration serviceability is increasingly seen to govern the design of FRP bridges and is more crucial than in the design of similar structures made of conventional construction materials [5]. In this paper, we refer to steel, concrete, steel-concrete composites and timber as the "conventional construction materials".

An obstacle to a wider use of FRP materials in structural engineering is the current lack of nationally or internationally recognised design standards [5,6]. Although there are guidelines and pre-standards for designers [7–11], they are mainly focused on static design. There are no tailored specifications for vibration serviceability design, except for a few recommendations adapted from the design standards for conventional construction materials, e.g. by limiting the static defection or fundamental frequency [9,11]. The dynamic properties (fundamental frequency, damping ratio, modal mass and mode shape) of FRP structures and their performance under dynamic actions (such as pedestrian excitation, vehicle loading, wind and train buffeting) need to be comprehensively studied to enable achievement of the full economic, architectural and engineering merits in having FRP components/structures.

This paper provides new experimental data on the dynamic properties of eight as-built FRP footbridges in Europe, created from tests conducted by the authors. In addition, it presents a comprehensive comparison of dynamic properties between FRP and non-FRP footbridges built after 1991 (for modern non-FRP footbridges), and provides a discussion on the similarities and differences of expected vibration responses. The comparison is based on the new experimental data presented herein, as well as for six other FRP footbridges and 124 modern non-FRP footbridges reported in the literature. In addition, the amplitude dependency of natural frequencies and damping ratios of two tested FRP footbridges is evaluated. Moreover, the accelerance peaks in

* Corresponding author at: School of Civil Engineering, Central South University, Changsha 410075, China.
E-mail address: xiaojun.wei@csu.edu.cn (X. Wei).

https://doi.org/10.1016/j.compstruct.2019.110956
Received 11 January 2019; Received in revised form 30 March 2019; Accepted 2 May 2019
Available online 03 May 2019
0263-8223/

the vertical direction are compared between FRP and conventional footbridges. The study reported in the paper offers crucial missing knowledge and the understanding required for us to have reliable design of FRP footbridges, and it can support the preparation of national or international consensus design guidance for dynamic design.

Following this introductory section, Section 2 describes the eight FRP footbridges tested by the authors. Section 3 details the modal testing and modal parameter identification carried out. Section 4 is used to demonstrate the amplitude-dependence of frequency and damping ratio. The comparison of fundamental frequencies and damping ratios of FRP and non-FRP footbridges is made in Section 5, while the comparison of accelerance peaks of FRP footbridges and conventional footbridges is made in Section 6. Concluding remarks from the research work are given in Section 7.

2. Description of FRP footbridges

Introduced in this section are eight as-built FRP composite footbridges, five in the UK, two in the Netherlands and one in Italy. In terms of structural form these footbridges consist of four girder bridges, two truss bridges and two suspension bridges. Unless otherwise stated the FRP material has glass fibre reinforcement embedded in a thermoset matrix, usually from the polyester resin family.

2.1. Parson's bridge

Fig. 1(a) and (b) show Parson's Bridge, an all-FRP structure located near to Aberystwyth in Wales [4]. This footbridge comprises of a square box cross-section 0.78 m wide by 0.78 m deep and 16.9 m long. It has FRP handrails as seen in the photographs. The square box is constructed of the Advanced Composites Construction System (ACCS), now pultruded in the USA by Strongwell. The total mass is around 1800 kg. Because of difficulties with site access, the superstructure was transported into a steep-sided valley by a non-military helicopter. This requirement limited the weight of the footbridge and is why FRP was chosen as the construction material. Parson's Bridge has been part of a public footpath across the countryside since 1995.

2.2. St. Austell bridge

St. Austell Bridge is the first all-FRP structure on the UK rail network [12] and was fabricated in 2007. It crosses over the Paddington-Penzance railway line near St. Austell station, Cornwall, England. The footbridge comprises of three spans of 5 m, 14 m and 6 m and is supported by existing masonry piers and abutments, as shown in Fig. 2(a) and (b). The width of the deck is 1.42 m. The structure, has a 'U' cross-section, of pultruded elements fabricated using the ACCS (as is Parson's Bridge in Section 2.1), with an outer moulded FRP shell, which is seen in the photographs. The central 14 m span has a mass of about 5000 kg.

2.3. Delft bridge A

Fig. 3(a) and (b) are for the Delft Bridge A, which is a footbridge of two spans of 15 m and 10 m, located on the campus of TU Delft, the Netherlands [13]. The FRP deck is 2 m wide and was moulded together with two longitudinal FRP beams underneath. The three components are of vacuum infused FRPs with a foam inner core. To support the footbridge, the two girders sit on neoprene pads at the span ends. The deck is surfaced with an epoxy layer with embedded gravel. The two spans are linked only by a steel bolted moment-free connection. Fig. 3 shows there are 1 m high steel handrails continuously along the two joined spans. The 15 m span weighs approximately 4500 kg.

2.4. Delft bridge B

The Delft Bridge B shown in Fig. 4 is 14.9 m long and 4.5 m wide, and was designed to take pedestrians, cyclists and a 12 tonnes service vehicle [13]. It crosses over a canal in the municipality of Delft, the Netherlands. The load-bearing structure is slightly cambered and it consists of four FRP longitudinal beams connected using an FRP cover to form the superstructure. Each beam is made using vacuum infused FRP with a foam inner core, thereby having a similar construction to Delft Bridge A, introduced in Section 2.3. The footbridge supports rest on neoprene pads, which also provide longitudinal restraint. The FRP handrail system is 1 m high and consists of individual vertical uprights as seen in Fig. 4. Using two steel bolts they are connected to the deck at 100 mm spacing. The total mass is around 6600 kg.

2.5. Dover Seawall Wellards Way

Dover Seawall Wellards Way, shown in Fig. 5(a) and (b), is located near the coastal town of Dover, England. This FRP footbridge provides pedestrian-only access to a beach. It consists of two 14.5 m simply-supported FRP truss footbridges, one of which is over the Dover to Folkstone Railway Line [14]. This bridge, installed in January 2017, replaces a steel bridge after a section of railway line was damaged by flooding. The superstructure is made of pultruded shapes (3.325 m high truss) and infused FRP sections with a foam inner core (2.4 m wide deck and parapet panels), bolted and bonded together. The 1.5 m high parapet panels were designed as a modular system and bolted to the truss members. The mass of each span is around 5500 kg.

(a) (b)

Fig. 1. Photographs of Parson's Bridge: (a) side view; (b) deck view.

(a) (b)

Fig. 2. Photographs of St. Austell Bridge: (a) side view; (b) deck view.

(a) (b)

Fig. 3. Photographs of Delft Bridge A: (a) side view; (b) deck view.

Fig. 4. Photograph of Delft Bridge B.

2.6. Prato Bridge

The Prato Bridge is a 25 m simply supported truss footbridge for pedestrians and cyclists, opened in 2008 [15,16]. As seen in Fig. 6(a) it crosses a dual carriageway in Prato, Italy. Fig. 6(b) shows the trusses, which are of pultruded FRP channel shapes. Stainless steel bolted connections have gusset plates of stainless steel. The deck is 2.5 m wide at the middle and 3.6 m at the span ends, and is assembled of pultruded FRP planks, which are each 5 m long and 500 mm wide and 40 mm deep. These planks are bolted at the ends, as well as at their mid-span to transverse members of channel shapes below the deck. The FRP planks themselves provide additional lateral bracing into the structure. Seen in Fig. 6(b) is the metal mesh that provides a barrier (for a hand rail) along the sides of the Prato Bridge. The structure weighs about 8000 kg [16], and rests on two concrete piers (Fig. 6a), each of 5.7 m height.

2.7. Wilcott Bridge

Wilcott Bridge, shown in Fig. 7(a) and (b) has been opened since 2003. It is a single span suspension footbridge over the Nesscliffe A5 bypass road [17,18], near to the English town of Shrewsbury. It has a deck width of 2.1 m and a span of 51.3 m. It consists of an FRP deck, two pairs of inclined steel pylons, two steel cables, and four steel backstays and 20 steel hangers (with 10 per side). The FRP deck is built in three units, using the ACCS systems, of approximately equal lengths that are connected by bonded interlocking splice joints. The 51 m long deck is integrally connected to the foundations, thereby removing the need for thermal-expansion movement joints. Ballast is employed to increase the mass of the deck. The deck structure including the ballast weighs around 31,000 kg.

2.8. Halgavor Bridge

The Halgavor Bridge, shown in Fig. 8(a) and (b), is a single span suspension footbridge over the A30 dual carriageway in the South of Bodmin, Cornwall, England [19]. This FRP footbridge, completed in 2001, is the first publicly funded bridge in the UK to use FRP as the

(a) (b)

Fig. 5. Photographs of Dover Bridge: (a) side view; (b) deck view.

principal material. The structure has a width of 3.5 m and a span of 47 m. It consists of a lightweight FRP deck, two pairs of steel pylons, two inclined steel cables, and four steel backstays, 20 steel hangers (10 per side) and parapet posts of a radial pattern. The FRP deck is fabricated from hand laid and vacuum infused components of fibres embedded in a vinylester resin matrix. The deck surface is made from recycled car tyres. The deck structure weighs about 8600 kg.

3. Modal testing and parameter identification of FRP footbridges

Table 1 summarises the essential dynamic testing and analysis details in our FRP footbridge test programmes. Five of these bridges were characterised for their dynamic properties using the impact hammer (IH) testing method, while the other three bridges were characterised using the ambient vibration (AV) testing method [20]. The IH testing method was chosen for the footbridges with spans below 20 m, while AV was employed for the footbridges with longer span. The key reason for employing IH is that the response of the shorter structures to ambient excitation is too low to acquire good quality AV data [21].

To identify the first few vibration modes of interest, a sufficiently dense grid of test points (TPs) on the deck is essential. The test programme for each bridge was divided into several set-ups, to cover the required test grid using the limited number of accelerometers available. The IH impact point on the deck remained unchanged. The measured force signal served as the reference signal. In AV testing, the signal from the accelerometer that remained in one location throughout served as the reference signal. The reference point on each bridge was carefully identified by preliminary tests so that the targeted vibration modes were observable.

In total three types of accelerometers were used for vibration response measurement, including the: Honeywell QA750 with nominal sensitivity 1300 mV/g (Fig. 9(a)); PCB 393C accelerometer with nominal sensitivity of 1000 mV/g (Fig. 9(b)); Dytran accelerometer 3166B1 with nominal sensitivity of 500 mV/g (Fig. 9(c)). A signal conditioner is required only when QA750 accelerometers are employed. Either a four-channel SignalCalc Quattro by Data Physics (shown in Fig. 10(a)) or a sixteen-channel SignalCalc Mobilyser by Data Physics (shown in Fig. 10(b)) was utilised for signal acquisition in real time.

In IH testing, the hammer operator, crouching on the deck, operated an instrumented hammer to impact the reference TP. The force signals were measured using a load cell embedded in the hammer and the resultant vibrations in the structure were measured using the accelerometers. The two hammers used were a Dytran Model 5803A (sensitivity 0.231 mV/N and weight 5.5 kg) or a Dytran Model 5802A (sensitivity 0.215 mV/N and weight 1.4 kg). The hammers are shown in Fig. 11(a), and (b), respectively. The typical force duration ranged from 4 ms to 7 ms. In order to minimise noise effects and leakage, a rectangular force window of 240 ms (for Parson's Bridge and Dover Bridge), 192 ms (for Delft Bridge A and Delft Bridge B) or 120 ms (for St. Austell Bridge) was applied to the input channel. Artificial damping of 0.0332 Hz (equivalent to a damping ratio of value 0.0332 (Hz)/the natural frequency (Hz) of a mode) was introduced by applying an exponential window to both force and response channels when testing Parson's Bridge, Delft Bridge A and Delft Bridge B [22]. In addition, measurements were repeated in each set-up to average out inherent noise. The recorded input force and output accelerations were used to construct and update frequency response functions, which become stable after six to eight repetitions. The resultant frequency response functions were then analysed by the Global Rational Fraction Polynomial (GRFP) method integrated in ME'scope 6.0 [23] to identify

(a) (b)

Fig. 6. Photographs of Prato Bridge: (a) side view; (b) deck view.

(a) (b)

Fig. 7. Photographs of Wilcott Bridge: (a) side view; (b) deck view.

modal parameters. The artificial damping that was introduced by the applied exponential window was eliminated during modal parameter identification [22].

By contrast, in AV testing, only vibration responses were measured under the natural excitation of wind and/or road traffic passing underneath. During data recording the footbridge had to be closed to pedestrian traffic. A reference-based data-driven Stochastic Sub-space Identification (SSI) algorithm, available in MACEC 3.2 [24–27], is applied for data pre-processing and modal parameter identification.

For the five FRP footbridges with spans < 20 m, the modes up to 20 Hz were identified. The modes below 10 Hz were identified for the Prato Bridge and the modes below 5 Hz for the two suspension bridges. Identified vibration modes are summarised in Table 2 and the description of mode shapes is related to the modal displacement of the deck, unless stated otherwise. Note that test results from the IH testing are related to the hammer operator-structure system rather than the structure itself [28–31]. The presence of hammer operator imposes an obvious influence on the dynamic properties of Parson's Bridge and Delft Bridge A, but a negligible influence for St Austell Bridge, Dover Bridge and Delft Bridge B. The hammer-operator influence on damping is known to be stronger than on changing the fundamental frequency. In Table 2 corrected values for the relevant modes for Parson's Bridge and Delft Bridge A are given in brackets. The detailed correction procedure can be found in [31].

For the five FRP footbridges with spans < 20 m, the fundamental frequency of the first vertical or torsional mode is well beyond the frequency range of 1.4 Hz–2.5 Hz for the first harmonic of dynamic force generated by pedestrian walking. Damping ratios for all the modes are ≥1.0%, except for 0.65%, for the first vertical mode of Delft Bridge A, and 0.8% for the first torsion mode of Dover Seawall Wellards Way. For the Prato Bridge, there is the first vibration mode at 2.05 Hz in the frequency range of the first forcing harmonic, but this mode is difficult to excite (most likely due to being dominated by the deflection of the top chord of the truss and comparatively small movement of the deck). There is a relatively high mode density in the frequency range 0–5 Hz for the two suspension bridges. The two vertical bending modes at 1.51 Hz and 2.21 Hz for Wilcott Bridge are potentially excitable by the first harmonic of walking force. Similar conclusion applies to Halgavor Bridge, owing to the presence of the two vertical bending modes at 1.91 Hz and 1.99 Hz, and a torsional mode at 2.03 Hz. The damping ratios of Wilcott Bridge are ≥0.8%, except for the exceptionally low damping ratio of 0.3% for the first lateral mode. For Halgavor Bridge, the damping ratios of the first three vertical bending modes are ≥1.1%, whilst the damping ratios of all the other modes are no lower than 0.3%.

4. Amplitude-dependence of frequency and damping ratio

Damping and natural frequencies of low-frequency modes of actual engineering structures are known to usually be response amplitude dependent [32–35], which is due to inherent nonlinearities, including effects from frictional forces at connections and supports, geometrical non-linearity, substructure-soil interaction or structural damages and so on. Fundamental frequencies and damping ratios of a footbridge estimated using the data obtained from vibration tests, in which induced vibration responses are usually at a relatively low level, might therefore

(a) (b)

Fig. 8. Photographs of Halgavor Bridge: (a) side view; (b) deck view.

Table 1
Modal testing and analysis methods for the eight bridges.

Bridge	Testing method	Excitation	Accelerometer	Data logger	Sampling frequency (Hz)	Window length (s)	Force window (ms)	Force duration (ms)	Artificial damping (Hz)	Identification method
Parsons Bridge	IH	Hammer (5803A)	QA750	Quattro	512	8	240	7	0.0332	GRFP
St. Austell Bridge	IH	Hammer (5802A)	QA750	Mobilyser	2048	4	120	7	0	GRFP
Delft Bridge A	IH	Hammer (5803A)	QA750	Quattro	1280	6.4	192	4	0.0332	GRFP
Delft Bridge B	IH	Hammer (5803A)	QA750	Quattro	1280	6.4	192	4	0.0332	GRFP
Dover Bridge	IH	Hammer (5803A)	QA750	Mobilyser	1024	8	240	5	0	GRFP
Prato Bridge	AV	Ambient excitation	PCB 393C and Dytran 3166B1	Quattro	256	600	N/A	N/A	N/A	SSI
Wilcott Bridge	AV	Ambient excitation	QA750	Mobilyser	256	1200	N/A	N/A	N/A	SSI
Halgavor Bridge	AV	Ambient excitation	QA750	Mobilyser	256	900	N/A	N/A	N/A	SSI

N/A: Not applicable; IH: Impact hammer testing; AV: Ambient vibration testing; GRFP: Global rational fraction polynominal; SSI: Stochastic sub-space identification.

be quite different from those of the bridge under its actual operational condition. Indeed, the estimation of fundamental frequency and damping ratio over an operating range of response amplitude is more important for estimating actual vibration performance.

To determine amplitude-dependency of the natural frequency and damping ratio for a targeted vibration mode, the free vibration response was measured under a human walking or jumping on a bridge to excite a targeted mode, as much as is practical. Then the logarithmic decrement method [36] is used to extract the required dynamic properties. Free decay tests were only successful on Parson's Bridge, Delft Bridge A and Wilcott Bridge although efforts were made on every bridge. For the sake of saving space, the authors exemplify the results from tests on both Parson's Bridge and Wilcott Bridge in this section.

4.1. Parson's Bridge

A pedestrian jumped at the mid-span and then jumped off the Parson's Bridge (introduced in Section 2.1 and Table 2) at 2.4 Hz, controlled by a metronome, aiming at exciting the first vertical bending mode with the 2nd forcing harmonic. The free decay of the vertical response at the mid-span, obtained after the pedestrian left the footbridge and band-pass filtered with a second order Butterworth filter with cut-off frequencies of 4.3 Hz and 5.3 Hz, is shown in Fig. 12. With change in acceleration peak from 0.16 to 4.31 m/s^2 Fig. 13(a) and (b) plot changes in fundament frequency and damping ratio. As the amplitude of acceleration increases from 0.16 m/s^2 to 4.31 m/s^2, the fundament frequency decreases from 4.81 Hz to 4.46 Hz (7.3%), whilst the damping ratio first increases from 2.16% to 2.46% and then decreases to 1.77%.

In IH testing, the vibration response for the first vertical mode at the mid-span has an acceleration up to 0.2 m/s^2, and the identified frequency and damping ratio are 4.75 Hz and 2.3%, respectively (bracketed results in Table 2). These values agree well with the frequency and damping ratio read from Fig. 13(a) and (b), respectively.

4.2. Wilcott Bridge

The vertical acceleration of Wilcott Bridge was measured, induced by a pedestrian walking over the bridge at 2.2 Hz, exciting the third vertical bending mode (see Table 2). Fig. 14 shows for the free decay at the quarter-span, filtered with a second order Butterworth filter having cut-off frequencies 2.0 Hz and 2.4 Hz. The corresponding frequency- and damping ratio-acceleration peak changes are presented in Fig. 15(a) and (b), respectively. Two types of nonlinearity can be observed from inspecting the results in the frequency-acceleration peak curve. With acceleration response amplitudes up to 0.13 m/s^2 (vertical lines in Fig. 15), the frequency increases with the peak value and the structure exhibits hardening non-linearity [37]. In contrast, this FRP footbridge exhibits a softening non-linearity [37] when acceleration peak is > 0.13 m/s^2. There is a corresponding dramatic change in damping ratio either side of 0.13 m/s^2, as shown in Fig. 15(b). The ambient vibration response, filtered with the same filter, has a peak of about 0.05 m/s^2, which suggests the fundamental frequency and damping ratio under natural excitation are 2.18 Hz and 1.0%. These results correlate strongly with the fundamental frequency of 2.21 Hz and damping ratio of 1.0% stated in Table 2. In addition, efforts were made during the test programme to excite other modes by using human-induced excitation. The outcome of these excitation exercises was that no useful free decay results could be achieved.

5. Comparison of dynamic properties of FRP and non-FRP footbridges

This section compares the dynamic properties of 14 FRP footbridges (i.e. the eight structures introduced in Sections 2 and 3 with six more having dynamic results reported in the literature [3,38–42]), with 124

(a) (b) (c)

Fig. 9. Accelerometers: (a) Honeywell QA750; (b) PCB 393C; (c) Dytran 3166B1.

non-FRP footbridges that were built after 1991. The modern non-FRP group includes data for 67 steel bridges [43–63], 38 concrete bridges [48,63–70], 13 steel-concrete composite bridges [46,60,68,71–79], five timber bridges [63,80–83] and one aluminium bridge [19]. Summarised in the Appendix table is the information for 51 of these 124 non-FRP footbridges to include: bridge description; test method; measured fundamental frequency and damping ratio of the first vertical mode. The Appendix table also has the same engineering information for 14 FRP footbridges. Bridge description and measured fundamental frequency of the remaining 73 non-FRP footbridges used in the comparison evaluation can be found in Ref. [63].

The table in the Appendix has eleven column headers, which are for: footbridge number; name; country of location; description for form of bridge; year of construction; the girder material; span in metres; if known, the modal mass in tonnes; the fundamental frequency of vibration in Hz; the damping ratio; the test method used to measure the dynamic properties. Note that 11 conventional material bridges [64,65,67,69,71–73,82,83] and three FRP bridges [40,41], with the test method marked by OMA*, were tested by using the operational modal analysis method with the presence of excitation from pedestrians performing walking, running, jumping or bouncing. Therefore, the modal parameter results presented for these structures might have been influenced by the presence of people that move on the structure.

5.1. Fundamental frequency evaluation

Vibration serviceability design guidelines for non-FRP footbridges imply that the vibration issues will be avoided if a footbridge has fundamental vertical frequency above 5 Hz (Sétra [45]), 8 Hz (the BSI's UK National Annex to Eurocode 1 [84]), 12 Hz (ISO [85]). Among structural designers, the 5 Hz limit is considered most often since it ensures avoiding resonance excitation by the first two walking harmonics (i.e. 1.25–2.5 Hz and 2.5–5.0 Hz, respectively), which contains most excitation energy. The vibration serviceability guidelines for FRP footbridges (such as AASHTO Guide Specifications for Design of FRP Pedestrian Bridges [86] and HA Design of FRP Bridges and Highway Structures [11]) tend to adopt directly this minimum frequency limit.

Plotted for 124 non-FRP footbridges, using circle symbols, in Fig. 16 are the measured fundamental frequencies, in a vertical mode, against the main span lengths from 4.8 m to 230 m. The fundamental frequencies range from 0.42 Hz to 13.5 Hz, and their Cumulative Distribution Function (CDF) is plotted in Fig. 17. It is observed that 86.3% of the conventional footbridges have a fundamental frequency < 5 Hz. Only 13.7% of non-FRP footbridges have fundamental frequency > 5 Hz, and these are mainly for spans < 25 m. Although the population of tested bridges published in literature might be skewed towards lively bridges (otherwise there might not be much need to test them), they still convey the fact that increasingly slender, lightweight, modern design solutions have difficulty in ensuring exceedance of the 5 Hz limit in practice. Of non-FRP footbridges, 34% of the footbridges are potentially excitable by the first harmonic of the pedestrian-induced force and 40.3% by the second.

A best-fit function, in the form of $f_v = \frac{a}{L}$ (Hz) (where f_v is the fundamental frequency of the vertical mode (Hz), L is the main span in metres and a is the fitting coefficient (m·Hz)), is found using the trust-region-reflective algorithm [87] based on data from 123 non-FRP footbridges. Bridge No. 18 in the Appendix table (for the Brugge Footbridge [46]) was excluded from the analysis due to having an extremely short main-span of 4.8 m.

The function is

$$f_v = \frac{100.5}{L}(\text{Hz}) \tag{1}$$

with the 95% confidence interval for the fitting coefficient as (93.3,

(a) (b)

Fig. 10. Data loggers: (a) Quattro; (b) Mobilyser.

(a) (b)

Fig. 11. Instrumented hammers: (a) Dytran Model 5803A; (b) Dytran Model 5802A.

Table 2
Identified modal parameters of the eight bridges.

Bridge	Mode no.	Mode shape description	Modal mass (kg)	Frequency (Hz)	Damping (%)
Parson's Bridge	1	1st lateral bending		4.30	2.2
	2	1st vertical bending	645	4.88 (4.75)	3.4 (2.3)
	3	2nd lateral bending		12.30	2.3
	4	2nd vertical bending		15.10	2.9
St Austell Bridge	1	1st lateral bending of parapets; slight deck torsion		6.48	3.2
	2	1st vertical bending of deck	2674	11.93	1.8
	3	2nd lateral bending of parapets; slight deck torsion		15.91	2.1
	4	3rd lateral bending of parapets; slight deck torsion		18.22	1.9
Delft Bridge A	1	1st vertical bending	3161	4.81 (4.78)	1.2 (0.65)
	2	1st torsional		8.31	2.6
	3	2nd torsional		9.47	2.0
	4	3rd torsional		13.76	1.7
	5	2nd vertical bending		17.07	1.2
Delft Bridge B	1	1st vertical bending (longitudinal)	3260	6.12	7.9
	2	1st torsional		10.10	4.4
	3	2nd vertical bending (transverse)		17.10	1.0
	4	3rd vertical bending (longitudinal and transverse)		18.90	2.1
Dover Seawall Wellards Way	1	1st vertical bending	4870	15.10	1.4
	2	1st torsional		20.00	0.8
Prato Bridge	1	1st torsional		2.05	1.6
	2	2nd torsional		2.70	1.3
	3	3rd torsional		4.80	1.4
	4	1st lateral bending		5.80	1.8
	5	1st vertical bending		7.46	2.6
	6	2nd vertical bending		8.07	1.7
	7	4th torsional		9.30	1.2
Wilcott Bridge	1	1st vertical bending		0.96	2.5
	2	1st lateral bending		1.08	0.3
	3	2nd vertical bending		1.51	1.9
	4	2nd lateral bending		1.56	1.7
	5	3rd vertical bending		2.21	1.0
	6	4th vertical bending		2.71	1.9
	7	1st torsional		3.22	0.8
	8	5th vertical bending		3.86	1.4
	9	3rd lateral bending		4.11	1.3
Halgavor Bridge	1	1st vertical bending		1.91	2.3
	2	2nd vertical bending		1.99	1.5
	3	1st torsional		2.03	0.3
	4	2nd lateral bending		2.12	0.8
	5	2nd torsional		2.79	0.4
	6	3rd vertical bending		3.20	1.1
	7	3rd torsional		3.49	0.6
	8	4th vertical bending		3.88	0.3
	9	4th torsional		4.48	0.5
	10	5th torsional		4.89	0.5

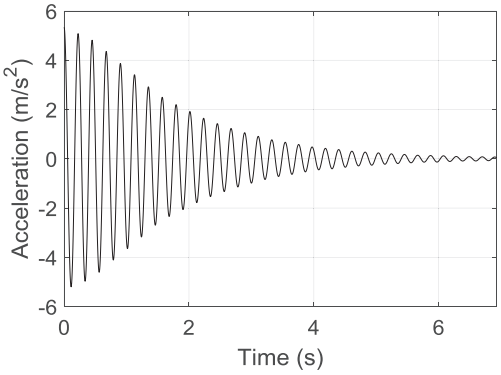

Fig. 12. Filtered free decay at the mid-span of the Parson's Bridge.

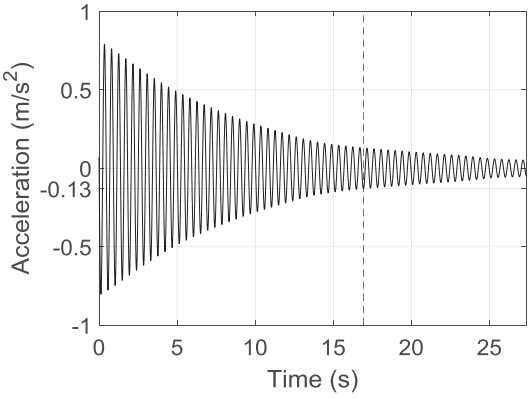

Fig. 14. Filtered free decay at the quarter-span of the Wilcott Bridge for mode at 2.2 Hz.

107.6). This best fit function is given by the solid line in Fig. 16. It offers a good representation to the mean measured data with a relatively high scatter in the span range of 20 to 50 m, resulting from the diverse variety of structural forms (see the Appendix table for descriptions of footbridge forms).

Using a cross symbol in Fig. 16 are displayed the measured fundamental frequencies of 14 FRP footbridges. It can be seen that, at the same spans, these FRP footbridges possess similar fundamental frequencies.

5.2. Damping ratio evaluation

Damping ratio is another important property for vibration analysis. The damping level of a structure is not only affected by the construction material, but also by the types of structural connections/joints and bridge bearings [32]. Damping ratios measured on full-scale footbridges are the most representative reference values for structural design. Bachmann *et al.* [88] summarised the damping ratios of 43 footbridges built before 1991, and they reported the average damping ratios for reinforced concrete, pre-stressed concrete, steel-concrete composite and steel footbridges to be 1.3%, 1.0%, 0.6% and 0.4%, respectively. In design guidelines for these footbridges, a particular damping ratio is usually recommended for vibration response analysis. In AASHTO Load Resistance Factor Design Bridge Design Specifications [89], 2%, 1% and 5% are suggested for the dynamic analyses of bridges of: concrete; welded and bolted steel; timber. In Eurocode 5 for timber [90], 1% and 1.5% damping ratios are recommended for footbridges without and with mechanical joints. Owing to limited experimental data from FRP footbridges, the 2016 Prospect for New Guidance in the Design of Fibre Reinforced Polymers [10] recommends an average damping ratio of 1.5% for a conservative lower limit for vibration serviceability analysis.

In the AASHTO Guide Specifications for Design of FRP Pedestrian Bridges [86], a damping ratio in the range 2%–5% is considered as more representative in structural analysis.

Presented in Fig. 18 are measured damping ratios with main span lengths for the first vertical modes for 44 out of the 124 non-FRP footbridges presented in Section 5.1. They are chosen because of the availability of measured damping ratio. As shown in the figure, using different symbols for the five construction materials, these 44 footbridges comprise 20 of steel (open-circle symbol) [44–52,56–62], eight of concrete (open-diamond symbol) [48,64–70], 12 of steel-concrete composite (star symbol) [46,60,68,71,72,74–79,91], three of timber (hexagram symbol) [80–82] and one of aluminium (diagonal cross symbol) [19]. In addition, the measured damping ratios of the 14 FRP footbridges described in Section 5.1 are introduced using a cross symbol to enable a comparison to be made. The range of damping ratios is from 0.14 to 7.9% and the range of spans from 4.8 to 173 m. It is observed that there is no obvious relationship between the damping ratio and main span length, which agrees with the finding of Tilly *et al.* [32]. Plotted in Fig. 19 are the CDFs for the five different construction materials. It can be seen that 75% of steel footbridges, 58% steel-concrete footbridges and 75% concrete footbridges have damping ratios $< 1\%$. In comparison, only 14% of FRP footbridges have damping ratios below 1% and 57% of FRP footbridges have a damping ratio $> 2\%$. It is noted that the damping ratio of the three timber footbridges range from 2.4% to 4.7%.

The mean, minimum and maximum damping ratios for footbridges of different construction materials are summarised in Table 3. The tabulated results show that at 0.85% steel footbridges have the lowest mean damping level, followed by 0.96% and 0.97% for concrete

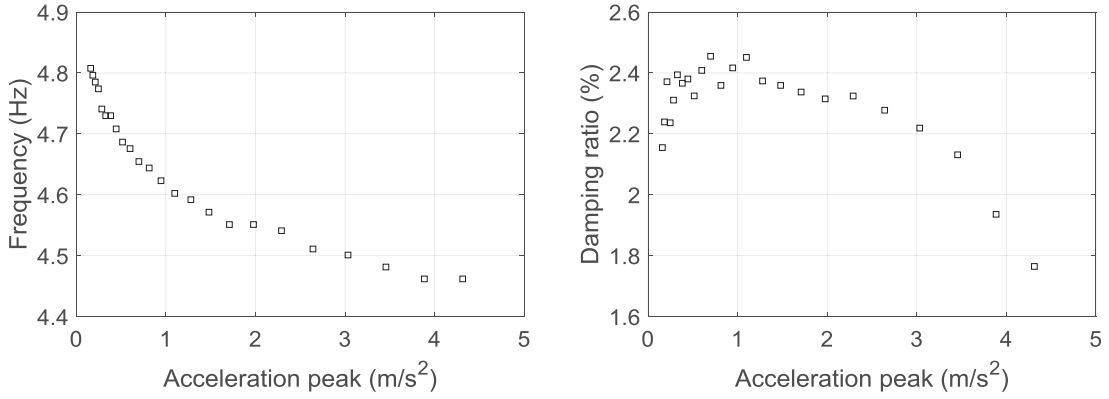

Fig. 13. (a) Frequency and (b) damping ratio against acceleration peak of the Parson's Bridge.

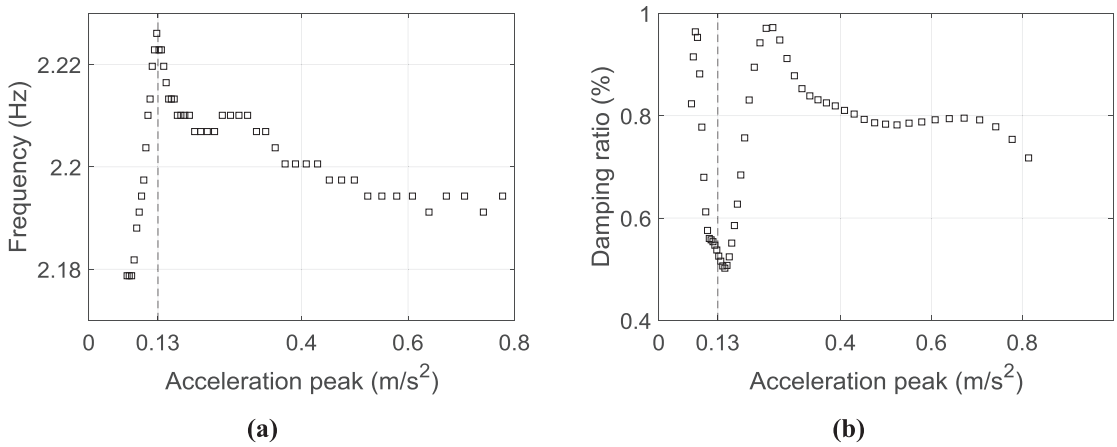

Fig. 15. (a) Frequency and (b) damping ratio against acceleration peak of the Wilcott Bridge for mode at 2.2 Hz.

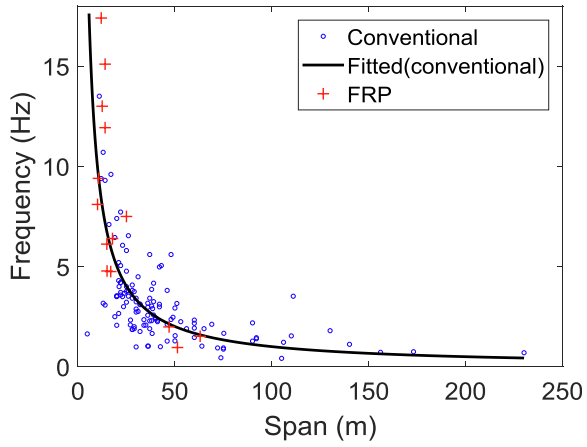

Fig. 16. Fundamental frequency versus main span.

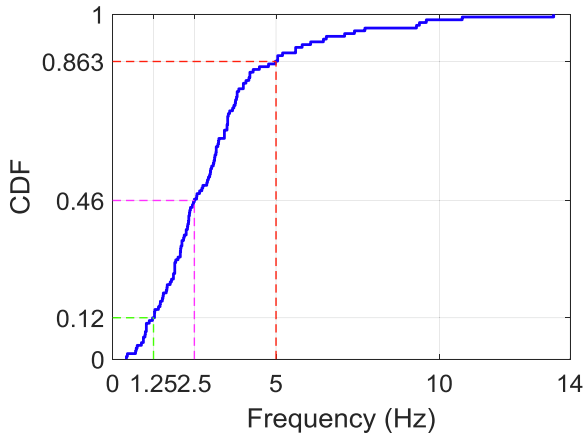

Fig. 17. CDF of fundamental frequencies of conventional footbridges.

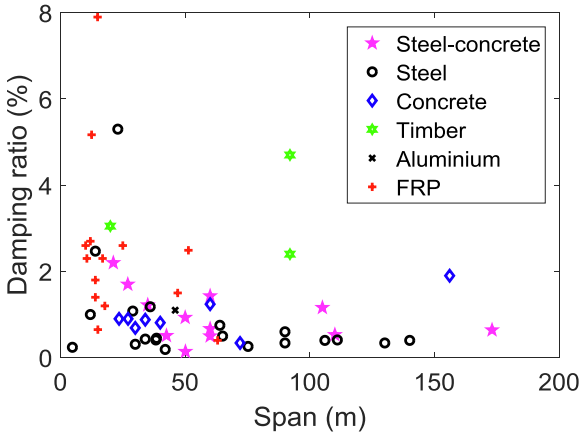

Fig. 18. Damping ratio versus main span.

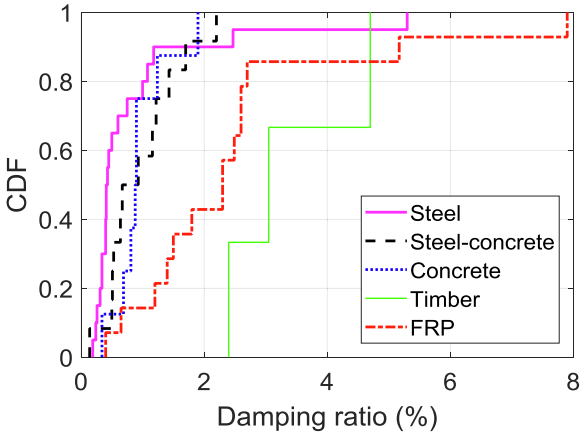

Fig. 19. CDFs of damping ratios of footbridges.

footbridges and steel-concrete footbridges. At over three times higher, timber footbridges have the highest mean damping level at 3.38%. For FRP footbridges the mean is 2.5%, with the widest range from 0.4% to 7.9%. The average damping levels of steel footbridges and steel-concrete composite footbridges reported herein are higher (by 113% and 62%, respectively) than those for bridges built before 1991 reported in a review by Bachmann *et al.* [88]. However, the average damping level of concrete footbridges at 0.86% is similar to the value for pre-stressed concrete footbridges and is lower than value for reinforced concrete bridges reported by Bachmann *et al.* [88]. Over the past three decades the mean damping ratios for steel, concrete and composite concrete-steel bridges have become more similar. The recommendations of the design guidelines that still propose use of different damping values for these three materials might therefore need to be updated to reflect this new reality.

6. Comparison of accelerance peaks of FRP and conventional footbridges

In this section a comparison is made between the accelerance peaks of FRP and conventional footbridges of the same bridge length, deck

Table 3
Damping ratios of the first vertical modes of footbridges of different materials.

Construction material	Damping ratio (%)		
	Mean	Min.	Max.
Steel	0.85	0.19	5.3
Concrete	0.96	0.34	1.9
Steel-concrete composite	0.97	0.14	2.2
FRP	2.50	0.4	7.9
Timber*	3.38	2.4	4.7

*: The results for timber category are for three bridges only.

width and mode shape.

The accelerance peak at the fundamental frequency f_v of a footbridge of given bridge length, deck width and mode shape can be approximately calculated as

$$A(f_v) \cong \frac{1}{2m\zeta} \ (\mathrm{m/s^2/N}) \tag{2}$$

where m is the modal mass and ζ is the damping ratio [92]. The fundamental frequency f_v can be determined from Eq. (1) for a given span length. The modal mass is proportional to the physical mass per square metre.

The representative values of physical mass per square metre for FRP and conventional footbridges are estimated using the data from ten FRP footbridges and nine conventional material footbridges. These 19 footbridges are in public use and they are chosen because of the availability of data on physical mass. Summarised in Tables 4 and 5 are their descriptions, for girder material, total length, main span length, width, total physical mass of girder structure and mass per square metre. The last columns in the two tables show that the average physical mass per square metre for the nine conventional footbridges is around 1200 kg/m^2 which is around 8.6 times higher than that of the ten FRP footbridges (around 140 kg/m^2). This means that the modal masses of conventional bridge will be 8.6 times larger than that for the FRP bridge of the same bridge length, deck width and mode shape.

According to Eq. (2), the accelerance peak at the fundamental frequency f_v of FRP bridge is 8.6 times larger than that for the non-FRP bridge of the same bridge length, deck width, damping ratio and mode shape. However, owing to a positive feature that the average damping value of FRP bridges is around 2.5 times larger (Table 3), the accelerance peak at the fundamental frequency f_v of FRP bridge is likely to be about 3.5 times larger. The same conclusion can be drawn for accelerance peaks at higher frequencies.

Given that FRP footbridges are found to be, on average, more responsive to dynamic loading by humans than conventional structures, there is strong possibility that their modes could be responsive to excitation by 3rd or even higher harmonics of the walking force. The minimum frequency limit of 5 Hz that is often deemed appropriate for conventional structures might be too low for FRP footbridges.

7. Concluding remarks

In this paper, we present new vibration testing and modal analysis results for eight FRP footbridges. A literature review has also been made to extract dynamic properties of 124 post-1991 non-FRP footbridges that are made of steel, concrete, steel-concrete composite, timber or aluminium, and six FRP footbridges. Comparing dynamic properties of 14 FRP footbridges with the non-FRP footbridges shows that fundamental frequencies at the same spans are independent of structural material. FRP footbridges are found to have, on average, a 2.5 times higher damping ratio for the first vertical mode than that of steel, concrete, and steel-concrete composite footbridges. However, they seem to have a lower damping ratio than timber footbridges. The frequencies and damping ratios of FRP footbridges identified from the measured free decay responses are found to be dependent on response amplitude. This amplitude dependence for natural frequency is likely to improve vibration performance of these bridges (compared with the alternative of amplitude-independent natural frequency) due to diffi-

Table 4
Structural parameters of ten FRP footbridges.

Number	Bridge name	Girder material	Total length (m)	Main span (m)	Width (m)	Total physical mass (kg)	Physical mass per square metre (kg/m^2)
1	Parsons Bridge	FRP	16.9	16.9	0.78	1800	137
2	St Austell Bridge	FRP	25	14	1.42	5000†	252
3	Delft Bridge A	FRP	20	15	2	4500†	150
4	Delft Bridge B	FRP	14.9	14.9	4.5	6600	98
5	Dover Seawall Wellards Way	FRP	29	14.5	2.4	5500†	158
6	Prato Bridge	FRP	25	25	2.5–3.6	8000	118
7	Wilcott Bridge	FRP	51.3	51.3	2.1	31000*	288
8	Halgavor Bridge	FRP	47	47	3.5	8600	52
9	Aberfeldy Bridge [3]	FRP	113	63	2.12	23000*	96
10	Pontresina Bridge	FRP	12.5	12.5	1.93	1680	70
						Average	142

*: Including ballast; †: Mass of the main span.

Table 5
Structural parameters of nine conventional footbridges.

Number	Bridge name	Girder material	Total length (m)	Main span (m)	Width (m)	Total physical mass (kg)	Physical mass per square metre (kg/m^2)
1	Changi Mezzanine Bridge [47]	Steel	200	140	4.2	1,300,000	1548
2	Cekov Footbridge [64]	Concrete	80	69	3	376,000	1567
3	Krakow Footbridge [64]	Concrete	80	40	4	472,000	1475
4	Baker Bridge [68]	Concrete	109	72	3	150,000	459
5	Stanisławice Footbridge [64]	Concrete	62	34	4.1	279,000	1098
6	Rotterdam Footbridge [76]	Steel-concrete	136	27	5.3	721,000	1000
7	Helix Bridge [57]	Steel	280	65	6	1,700,000	1012
8	Podgorica Bridge [3]	Steel	104	78	3	260,000	833
9	Noisy-le-Grand Footbridge [45]	Concrete	88	44	5	860,000	1955
						Average	1216

culties to develop resonance response when structural frequency is varying with amplitude. In addition, it is found that the accelerance peaks of FRP footbridges are, on average, about 3.5 times higher than those of conventional footbridges. We conclude that it may be inappropriate to use the minimum frequency limits from serviceability guidelines for conventional bridges, as is currently frequent practice, to ensure satisfying the vibration serviceability state in the design of FRP bridges. This study provides crucial missing technical information that is required for developing reliable design method for 'lightweight' FRP footbridges, and it will support the preparation of national and international consensus design guidance for their dynamic design.

Acknowledgements

The authors acknowledge the support of the UK Engineering and Physical Sciences Research (EPSRC) Council (Grant Number EP/M021505/1: Characterising dynamic performance of fibre reinforced polymer structures for resilience and sustainability). In addition, the authors acknowledge the technical and field-testing support from Mr Steve Jones, Mr Jonathan Meadows and Mr Neil Gillespie of the School of Engineering at the University of Warwick, Mr Casper Kruger from Pipex px®, Prof. Salvatore Russo and Dr Giosue Boscato of Iuav University of Venice and Alessandro Adilardi of Prato Municipality in Italy, and Dr Marko Pavlović of TU Delft, the Netherlands.

Data availability

The raw and processed data required to reproduce these findings can be found at http://wrap.warwick.ac.uk/117039.

Appendix. Dynamic properties of FRP and conventional material footbridges

Notes: OMA: Operational modal analysis; OMAX: OMA with eXogenous inputs; ST: Shaker testing; IH: Impact hammer testing; HST: Experimental modal analysis using human-induced force as input; OMA*: Operational modal analysis with the presence of excitation from active pedestrian(s) (e.g. from walking, jumping, running or bouncing); N/A: Not Available.

Steel footbridges

No	Name	Country	Description for form	Construction year	Girder material	Main span (m)	Modal mass (t)	Frequency (Hz)	Damping ratio (%)	Test methods
1	Postiguet Footbridge [43]	Spain	Continuous girder bridge with six spans of various length; Width: 2.2 m	1993	Steel	24	N/A	3.67	N/A	OMA
2	Zlotnicka Footbridge [44]	Poland	Cable stayed footbridge; Length: 68 m; Width: 3.0 m	1999	Steel	34	N/A	2.07	0.43	OMA
3	Solferino Footbridge without TMD damper [45]	France	Steel arch bridge; Length: 140 m; Width: 12–14.8 m; Weight: 900 t	1999	Steel	106	N/A	1.22	0.3–0.5	N/A
4	Eeklo Footbridge [46]	Belgium	Continuous steel bridge with U-shaped cross section; Length: 96 m; Width: 3 m	2002	Steel	42	N/A	2.99	0.19	OMA
5	Changi Mezzanine Bridge [47]	Singapore	A flat arch footbridge; Length: 200 m; Weight:1300 t	2002	Steel	140	402	1.12	0.4	ST
6	Wetteren Footbridge [48,49]	Belgium	A tied-arch bridge; Length: 105.5 m	2003	Steel	75.2	N/A	1.67	0.26	OMAX
7	Erzbahnschwinge Footbridge [50]	Germany	A suspension bridge with a S-shape; Width:3 m;	2003 [93]	Steel	130	N/A	1.80	0.34	N/A
8	Ninove Footbridge [46]	Belgium	Cable-stayed bridge with a steel truss girder; Length: 58.5 m	2004	Steel	36	N/A	2.97	1.18	OMA
9	Valladolid Footbridge [51]	Spain	A continuous truss bridge; Total length: 234 m	2004	Steel	111	N/A	3.52	0.41	OMA
10	Trabzon Footbridge A [52]	Turkey	A steel truss bridge; Length: 18.4 m; Width: 2.3 m	2006	Steel	12	N/A	9.39	1.0	OMA
11	Viana Footbridge [53]	Portugal	A movable cable-stayed bridge; Length: 44.7 m; Width: 2.5 m	2007	Steel	36.3	N/A	1.03	N/A	OMA
12	Weil-am-Rhein Footbridge [54,55]	Germany	Steel arch bridge; Length: 230 m; Width: 5–5.5 m	2007	Steel	230	N/A	0.7	N/A	OMA
13	Guarda Footbridge [56]	Portugal	Tied-arch footbridge of total length 123 m	2007	Steel	90	N/A	2.19	0.34	OMA
14	Leuven footbridge [46]	Belgium	Steel continuous girder bridge; Length: 23 m; Width: 5 m	2009	Steel	14	N/A	3.08	2.47	OMA
15	Anderlecht footbridge [46]	Belgium	Steel arch bridge; Length: 57 m; Width: 4.8 m	2010	Steel	30	N/A	3.24	0.31	OMA
16	Helix Bridge [57]	Singapore	Continuous girder bridge; Length: 280 m; Width: 6 m	2010	Steel	65	277	1.90	0.5	ST
17	Mechelen Footbridge [46]	Belgium	Steel bridge with L-shape cross section; Length: 31 m; Width:3 m	2011	Steel	29	N/A	3.75	1.08	OMA
18	Brugge Footbridge [46]	Belgium	Continuous steel bridge with L-shape cross section; Length: 57 m; Width:2.7 m	2012	Steel	4.8	N/A	1.64	0.24	OMA
19	Seriate Footbridge [58]	Italy	Suspension footbridge; Length: 63.9 m; Width: 2.5–5.0 m	2012	Steel	63.9	N/A	1.03	0.75	OMA
20	A41 All Saints Way Footbridge [59]	England	Cable stayed bridge; Length: 51.15 m	2012	Steel	38.5	N/A	2.9	0.45	OMA
21	Serra Footbridge [60]	Italy	Tied-arch bridge; Length: 120 m	2012	Steel	90	N/A	1.28	0.6	OMA
22	Bears' Cage Footbridge [61]	Belgium	Butterfly-shaped bridge; Length:23 m; Width: 4–14 m	2014	Steel	23	N/A	6.06	5.3	OMA
23	Charleroi Footbridge [62]	Belgium	A single span bridge; Length: 38.25 m; Width: 13.35 m	2014	Steel	38.25	N/A	1.66	0.41	OMA

Concrete footbridges

No	Name	Place	Description for form	Construction year	Material for the girder	Main span (m)	Modal mass (t)	Frequency (Hz)	Damping ratio (%)	Test methods
24	Cekov Footbridge [64]	Czech Republic	Arch bridge; Length:80 m; Width: 3 m; Weight: 376 t	1995	Concrete	69	N/A	2.12	N/A	OMA*
25	Sherbrooke Footbridge [65]	Canada	A post-tensioned space truss bridge; Length: 60 m; Width: 3.3 m	1997	Concrete	60	N/A	2.33	1.24	OMA*
26	FEUP Footbridge [48]	Portugal	Stress-ribbon footbridge; Length: 58 m; Width:3.8 m	1998	Concrete	30	N/A	0.99	0.69	OMAX
27	Reykjavik Footbridge A [66]	Iceland	Continuous girder bridge with a spiral shape; Length: 170 m; Width: 3.26 m	2005	Concrete	27.1	46	2.33	0.9	ST
28	Reykjavik Footbridge B [67]	Iceland	A 5-span continuous girder bridge; Length 86 m; Width: 3.26 m	2005	Concrete	23.5	N/A	3.0	0.9	OMA*
29	Krakow Footbridge [64]	Poland	Continuous girder bridge; Length: 80 m; Width:4 m; Weight:472 t	2005	Concrete	40	N/A	2.44	0.81	OMA
30	Baker Bridge [68]	England	Cable stayed footbridge; Length: 109 m; Width:3 m; Weight: 150 t	2007	Concrete	72	55.5	0.94	0.34	HST
31	Texas foot-bridge [69]	USA	A bridge of three simply supported pre-stressed reinforced concrete spans; Length: 109 m; Width 3.66 m	2008	Concrete	40	N/A	2.38	N/A	OMA*
32	Stanisławice Footbridge [64]	Poland	Continuous rigid frame footbridge with inclined piers; Length: 62 m; Width: 4.1 m; Weight: 279 t	2011	Concrete	34	N/A	2.35	0.88	OMA*
33	Celakovice Footbridge, [70]	Czech Republic	Cable-stayed footbridge; Length: 242 m; Width: 3.64 m	2014	Concrete	156	N/A	0.72	1.9	ST

Steel-concrete composite footbridges

No	Name	Place	Description for form	Construction year	Material for the girder	Main span (m)	Modal mass (t)	Frequency (Hz)	Damping ratio (%)	Test methods
34	Kochenhofsteg Footbridge [71]	Germany	A single span suspension bridge with an inclined mast; Length:42.5 m; Width: 3 m	1992	Steel-con-crete	42.5	N/A	1.0	0.51	OMA*
35	Eutinger Waagsteg Bridge [71,72]	Germany	A stress ribbon bridge; Length: 50 m; Width: 2.88 m	1991	Steel-con-crete	50	N/A	1.29	0.93	OMA*
36	Glacisbruecke in Minden [71,91]	Germany	A suspension bridge; Length: 138 m	1995	Steel-con-crete	105	N/A	0.42	1.16	OMA*
37	Katzbuckelbruecke bridge [71,73]	Germany	A movable suspension bridge; Length:73.7 m; Width: 3.5 m	1999	Steel-con-crete	73.7	N/A	0.45	N/A	OMA*
38	Trabzon Footbridge B [74]	Turkey	A tied-arch bridge; Length: 35 m; Width:3.3 m	2006	Steel-con-crete	35	N/A	2.08	1.22	OMA
39	Pedro e Inês foot-bridge [75]	Portugal	An arch bridge; Length: 275 m; Width: 4 m	2006	Steel-con-crete	110	N/A	1.54	0.53	OMA
40	Knokke footbridge [46]	Belgium	A cable stayed bridge; Length: 106 m; Width: 3 m	2008	Steel-con-crete	50.1	N/A	1.55	0.14	OMA
41	Rotterdam Footbridge [76]	Netherlands	A six-span simply supported girder bridge; Length: 136 m; Width: 5.3 m; Weight: 721 t	2007	Steel-con-crete	27	N/A	2.09	1.7	OMA
42	Pasternak Footbridge [77]	Italy	A cable stayed bridge with curved deck; Length: 270 m; Width:3 m	2008	Steel-con-crete	60	N/A	1.46	0.67	OMA
43	De Gasperi Footbridge [60]	Italy	A bridge with a steel arch supporting concrete deck; Length: 60 m; Width: 3 m	2010	Steel-con-crete	60	N/A	2.17	0.5	OMA
44	Ponte del Mare Footbridge (without dampers) [78]	Italy	A cable stayed bridge with two separate curved decks; Length (Width): 148 m (4.1 m) and 173 m (3.1) for cycle and foot track deck, respectively	2010	Steel-con-crete	173	N/A	0.75	0.64	OMA
45	Pcim Footbridge [79]	Poland	Cable-stayed bridge; Length: 111 m	2011	Steel-con-crete	60	N/A	1.95	1.46	OMA
46	Skybridge [68]	Singapore	Bridge over an atrium; Length: 21.2 m	2015	Steel	21.2	12.3	4.0	2.2	HST

Timber footbridges

No	Name	Place	Description for form	Construction year	Material for the girder	Main span (m)	Modal mass (t)	Frequency (Hz)	Damping ratio (%)	Test methods
47	Marecchia River Footbridge [80]	Italy	A laminated timber tied arch bridge; Length: 92 m; Width: 5 m	2000	Timber	92	N/A	1.4	4.7	ST
48	Lardal Bridge [81]	Norway	A glue-laminated timber arch bridge; Length: 130 m; Width: 2.4 m	2001	Timber	92	N/A	1.45	2.4	OMA or ST
49	Glentress Footbridge [82]	Scotland	A stress-laminated timber arch bridge; Length: 20 m; Width: 2–3 m	2004	Timber	20	N/A	3.54	3.05	OMA*
50	Pribor Footbridge [83]	Czech Republic	A cable stayed footbridge; Length: 43 m; Width: 3 m	2015	Timber	39	N/A	4.17	N/A	OMA*

Aluminium footbridges

No	Name	Place	Description for form	Construction year	Material for the girder	Main span (m)	Modal mass (t)	Frequency (Hz)	Damping ratio (%)	Test methods
51	Lockmeadow Bridge [19]	United Kingdom	A two-span cable-stayed footbridge; Length: 80 m; Width: 2.1 m; Weight: 26.4 t	1999	Aluminium	46	N/A	1.28	1.1	ST

FRP footbridges

No	Name	Place	Description for form	Construction year	Material for the girder	Main span (m)	Modal mass (t)	Frequency (Hz)	Damping ratio (%)	Test methods
52	Aberfeldy Bridge [3,38]	Scotland	A cable-stayed bridge; Length: 113 m; Width:2.12 m; Weight 23 t	1992	FRP	63	2.75	1.52	0.4	N/A
53	Parsons Bridge	Wales	A single span girder bridge; Length: 16.9 m; Width 0.78 m; Weight:1.8 t	1995	FRP	16.9	0.645	4.75	2.3	IH
54	Delft Bridge A	Netherlands	A two-span girder bridge; Length: 25; Width: 2 m; Weight: 4.5 t	2016 (Design)	FRP	15	3.161	4.78	0.65	IH
55	Delft Bridge B	Netherlands	A girder bridge; Length: 14.9 m; Width:4.5 m; Weight: 6.6 t	2015 (Design)	FRP	14.9	3.26	6.12	7.9	IH
56	Pontresina Bridge (Bonded) [39]	Switzerland	A removable truss bridge; Length:12.5 m; Width:1.93 m; Weight:1.68 t	1997	FRP	12.5	N/A	13	5.17	OMA
57	Halgavor Bridge	England	A suspension bridge; Length: 47 m; Width:3.5 m; Weight (deck): 8.6 t	2001	FRP	47	N/A	1.99	1.5	OMA
58	Wilcott Bridge	England	A suspension bridge; Length:51.3; Width:2.1 m; Weight (deck including ballast): 31 t	2003	FRP	51.3	N/A	0.96	2.49	OMA
59	St Austell Footbridge	England	A three-span simply supported bridge; Length: 25 m; Width: 1.42 m; Weight (14 m span): 5 t;	2007	FRP	14	2.674	11.93	1.8	IH
60	Hakui Bridge [40]	Japan	A single-span bridge; Length: 11.3 m; Width: 4 m	2008	FRP	10.6	N/A	9.4	2.3	OMA*
61	Tsukuba Bridge [40]	Japan	A single-span bridge; Length:10.8 m	2008	FRP	10.1	N/A	8.1	2.6	OMA*
62	Prato Bridge	Italy	A truss bridge; Length: 25 m, Width: 2.5–3.6 m; Weight: 8 t	2008	FRP	25	N/A	7.5	2.6	OMA
63	A Truss bridge [41]	Japan	A pony truss footbridge; Length:18.3 m; Width:2.0 m	No earlier than 2008	FRP	17.8	N/A	6.4	1.2	OMA*
64	Bradkirk Bridge [42]	England	A two-span bridge; Length: 24 m; Width: Weight (each span) < 2 t	2009	FRP	12	N/A	17.4	2.7	OMA
65	Dover Seawall Wellards Way	England	A two-span truss bridge; Length: 28	2017	FRP	14	2.675	15.1	1.4	IH

References

[1] Potyrała PB. Use of fibre reinforced polymers in bridge construction: state of the art in hybrid and all-composite structures [Master thesis] Universitat Politècnica de Catalunya; 2011.

[2] Wan B. Using fiber-reinforced polymer (FRP) composites in bridge construction and monitoring their performance: an overview. Adv Compos Bridge Constr Repair 2014:3–28.

[3] Živanović S, Feltrin G, Mottram JT, Brownjohn JMW. Vibration performance of bridges made of fibre reinforced polymer. Catbas FN, editor. Dynamics of civil structures, Volume 4. Springer International Publishing; 2014. p. 155–62.

[4] Živanović S, Wei X, Russell J, Mottram JT. Vibration performance of two FRP footbridge structures in the United Kingdom. Berlin, Germany: Footbridge 2017; 2017. 6–8 September.

[5] Ellingwood BR. Toward load and resistance factor design for fiber-reinforced polymer composite structures. J Struct Eng 2003;129:449–58.

[6] Mottram JT. Fibre reinforced polymer structures: Design guidance or guidance for designers. In: The 8th International Conference on Advanced Composites in Construction. Chesterfield, UK. 5-7 September, 2017.

[7] BÜV-Empfehlung. Tragende Kunststoffbauteile im Bauwesen [TKB] – Entwurf, Bemessung und Konstruktion. Wsebaden, Germany: Springer; 2014.

[8] CNR. Guide for the design and construction of structures made of FRP pultruded elements. Rome, Italy: Advisory Committee on Technical Recommendations for Construction, National Research of Italy; 2008.

[9] ASCE. Pre-standard for load and resistance factor design (LRFD) of pultruded fibre reinforced polymer (FRP) structures. Reston, VA: American Society of Civil Engineers; 2010.

[10] Ascione L, Caron J-F, Godonou P, Van IJselmuijden K, Knippers J, Mottram JT, *et al.* Prosepct for new guidance in the design of FRP. In: Ascione L, Gutierrez E, Silvia

Dimova, Pinto A, Denton S, editors.: EUR 27666 EN; 2016.
[11] HA. Design of FRP bridges and highway structures, Part 17, BD 90/05. Highways Agency 2005.
[12] Shave J, Denton S, Frostick I. Design of the St Austell fibre-reinforced polymer footbridge, UK. Struct Eng Int 2010;20:427–9.
[13] Živanović S, Russell J, Pavlović M, Wei X, Mottram JT. Effects of pedestrian excitation on two short-span FRP footbridges in Delft. Pakzad S, editor. Dynamics of civil structures, Volume 2. Cham: Springer International Publishing; 2019. p. 143–50.
[14] Russell J, Wei X, Živanović S, Kruger C. Dynamic response of an FRP footbridge due to pedestrians and train buffeting. Procedia Eng 2017;199:3059–64.
[15] Wei X, Boscato G, Russell J, Adilardi A, Russo S, Živanović S. Experimental characterisation of dynamic properties of an All-FRP truss bridge. Pakzad S, editor. Dynamics of civil structures, Volume 2. Cham: Springer International Publishing; 2019. p. 169–76.
[16] Adilardi A, Frasconi L. Design of a pedestrian bridge dade with pultruded profiles of fibreglass-reinforced plastics in Prato. In: The 3rd International Conference on Footbridges Porto, Portugal. 2–4 July, 2008.
[17] Wei X, Russell J, Živanović S, Mottram JT. Experimental investigation of the dynamic characteristics of a glass-FRP suspension footbridge. In: Caicedo J, Pakzad S, editors. Dynamics of civil structures, Volume 2: Proceedings of the 35th IMAC, A Conference and Exposition on Structural Dynamics. Cham: Springer International Publishing; 2017. p. 37–47.
[18] Votsis RA, Stratford TJ, Chyssanthopoulos MK. Dynamic assessment of a FRP suspension footbridge. In: The 4th International Conference on Advanced Composites in Construction. Edinburgh, United Kingdom. 1–3 September, 2009.
[19] Firth IPT. A tale of two bridges: the Lockmeadow and Halgavor Bridges. Struct Eng 2002;80:26–32.
[20] Ewins DJ. Modal testing: theory and practice. second ed. Baldock, Hertfordshire, England: Research Studies Press Ltd.; 2000.
[21] Cantieni R. Equipment and testing techniques for small to medium sized structures. In: The 26th International Modal Analysis Conference. Orlando, Florida, USA. 4–7 February, 2008.
[22] Fladung WA. Windows used for impact testing. In: The 5th International Modal Analysis Conference. London, England 6–9 April, 1987.
[23] ME'scope VES. ME'scope VES 6.0. Scotts Valley, CA: Vibrant Technology. Inc; 2013.
[24] Reynders E, Schevenels M, Roeck GD. MACEC 3.2: a matlab toolbox for experimental and operational modal analysis. KU Leuven: Department of Civil Engineering; 2014.
[25] Peeters B, De Roeck G. Reference-based stochastic subspace identification for output-only modal analysis. Mech Syst Sig Process 1999;13:855–78.
[26] Peeters B, De Roeck G. Stochastic system identification for operational modal analysis: a review. J Dyn Syst Meas Contr 2001;123:659–67.
[27] Reynders E, Roeck GD. Reference-based combined deterministic–stochastic subspace identification for experimental and operational modal analysis. Mech Syst Sig Process 2008;22:617–37.
[28] Wei X, Russell J, Živanović S, Mottram JT. The effects of hammer operator in manually operated impact hammer testing of lightweight structures. In: The 7th World Conference on Structural Control and Monitoring. Qingdao, China. 22–25 July, 2018.
[29] Wei X, Živanović S. Frequency response function-based explicit framework for dynamic identification in human-structure systems. J Sound Vib 2018;422:453–70.
[30] Wei X, Živanović S, Russell J, Mottershead JE. Subsystem identification in structures with a human occupant based on composite frequency response functions. Mech Syst Sig Process 2019;120:290–307.
[31] Wei X, Živanović S, Huang T, He X. Correction of the influence of the hammer operator in impact hammer tests of two FRP footbridges. Eng Struct 2019.
[32] Tilly GP, Cullington DW, Eyre R. Dynamic behaviour of footbridges. IABSE Surveys S-26/84. IABSE Periodica 1984:13–24.
[33] Tamura Y, Suganuma S-Y. Evaluation of amplitude-dependent damping and natural frequency of buildings during strong winds. J Wind Eng Ind Aerodyn 1996;59:115–30.
[34] Brownjohn JMW, Fu TN. Vibration excitation and control of a pedestrian walkway by individuals and crowds. Shock Vib 2005;12.
[35] Chen G-W, Beskhyroun S, Omenzetter P. Experimental investigation into amplitude-dependent modal properties of an eleven-span motorway bridge. Eng Struct 2016;107:80–100.
[36] Inman DJ. Engineering vibration. Upper Saddle, NJ: Pearson Education Inc; 2008.
[37] Worden K, Tomlinson GR. Nonlinearity in structural dynamics: detection, identification and modeling. CRC Press; 2000.
[38] Cadei J, Stratford T. The design, construction and in-service performance of the all-composite Aberfeldy footbridge. Advanced polymer composites for structural applications in construction. ICE Publishing; 2002. p. 445–53.
[39] Bai Y, Keller T. Modal parameter identification for a GFRP pedestrian bridge. Compos Struct 2008;82:90–100.
[40] Fukuda S, Kajikawa Y, Nishizaki I, Kishima T, Hosonuma H. Vibration characteristics and serviceability of the FRP girder bridge. In: The 2nd International Multi-Conference on Complexity, Informatics and Cybernetics. Orlando, Florida. March, 2011.
[41] Kumada T, Yamada S, Johansen E, Wilson R. Static and dynamic behavior of a pultruded FRP truss footbridge. In: The 2nd Official International Conference of International Institute for FRP in Construction for Asia-Pacific Region. Seoul Korea. 9-11 December 2009.
[42] dos Santos FM, Mohan M. Train buffeting measurements on a fibre-reinforced plastic composite footbridge. Struct Eng Int 2011;21:285–9.
[43] Ivorra S, Foti D, Bru D, Baeza FJ. Dynamic behavior of a pedestrian bridge in Alicante, Spain. J Perform Constr Facil 2015;29:04014132.
[44] Hawryszków P, Pimentel R, Silva F. Vibration effects of loads due to groups crossing a lively footbridge. Procedia Eng 2017;199:2808–13.
[45] Sétra. Footbridges. Assessment of vibrational behaviour of footbridges under pedestrian loading. The Technical Department for Transport, Roads and Bridges Engineering and Road Safety 2006.
[46] Van Nimmen K, Lombaert G, De Roeck G, Van den Broeck P. Vibration serviceability of footbridges: evaluation of the current codes of practice. Eng Struct 2014;59:448–61.
[47] Brownjohn J, Fok P, Roche M, Moyo P. Long span steel pedestrian bridge at Singapore Changi Airport-part 1: prediction of vibration serviceability problems. Struct Eng 2004;82:21–7.
[48] Reynders E, Degrauwe D, De Roeck G, Magalhães F, Caetano E. Combined experimental-operational modal testing of footbridges. J Eng Mech 2010;136:687–96.
[49] Reynders E, Houbrechts J, De Roeck G. Fully automated (operational) modal analysis. Mech Syst Sig Process 2012;29:228–50.
[50] Kasperski M. Vibration serviceability for pedestrian bridges. Proc Inst Civ Eng Struct Build 2006;159:273–82.
[51] de Sebastian J, Díaz I, Casado C, Vasallo A, Poncela A, Lorenzana A. Environmental and crowd influence on the dynamic behaviour of an in-service footbridge. In: The 4th International Conference on Footbridge. Wroclaw, Poland. 6–8 July, 2011.
[52] Bayraktar A, Altunişik AC, Sevim B, Türker T. Ambient vibration tests of a steel footbridge. J Nondestr Eval 2010;29:14–24.
[53] Barbosa R, Magalhães F, Caetano E, Cunha Á. The Viana footbridge: construction and dynamic monitoring. Proc Inst Civ Eng Bridge Eng 2013;166:273–90.
[54] Ingólfsson ET, Georgakis CT, Jönsson J. Pedestrian-induced lateral vibrations of footbridges: a literature review. Eng Struct 2012;45:21–52.
[55] Mistler M, Heiland D. Lock-in-Effekt bei Brücken infolge FuSSgängeranregung – Schwingungstest der weltlängsten FuSSgänger- und Velobrücke (lock-in effect due to pedestrian excitation of bridges – vibration test of the world's longest pedestrian and bicycle bridge). D-A-CH Tagung. Vienna, Austria. September, 2007.
[56] Pimenta H, Rebelo C, Rigueiro C. Experimental Tests on the Guarda Footbridge. In: The 3rd International Conference on Footbridges. Porto, Portugal. 2–4 July, 2008.
[57] Brownjohn JMW, Reynolds P, Fok P. Vibration serviceability of Helix Bridge, Singapore. Proc Inst Civ Eng Struct Build 2016;169:611–24.
[58] Lai E, Gentile C, Mulas MG. Experimental and numerical serviceability assessment of a steel suspension footbridge. J Constr Steel Res 2017;132:16–28.
[59] Modalyse. Modal properties and vibration characteristics of footbridge. http://modalyse.com/footbridge-measure/ [accessed 04 December 2018].
[60] Tubino F, Carassale L, Piccardo G. Human-induced vibrations on two lively footbridges in Milan. J Bridge Eng 2016;21:C4015002.
[61] Van Nimmen K, Van den Broeck P, Verbeke P, Schauvliege C, Mallié M, Ney L, et al. Numerical and experimental analysis of the vibration serviceability of the Bears' Cage footbridge. Struct Infrastruct Eng 2017;13:390–400.
[62] Van Nimmen K, Verbeke P, Lombaert G, De Roeck G, Van den Broeck P. Numerical and experimental evaluation of the dynamic performance of a footbridge with tuned mass dampers. J Bridge Eng 2016;21:C4016001.
[63] Oliveira C. Fundamental frequencies of vibration of footbridges in Portugal: from in situ measurements to numerical modelling. Shock Vib 2014;2014:1–22.
[64] Pantak M. Dynamic characteristic of the medium span concrete footbridges. J Civ Eng Arch 2014;8:1445–52.
[65] Paultre P, Proulx J, Légeron F, Le Moine M, Roy N. Dynamic testing of the Sherbrooke Pedestrian Bridge. IABSE Congress Report: International Association for Bridge and Structural Engineering; 2000. p. 1254–61.
[66] Živanović S, Ingólfsson ET, Pavić A, Gudmundsson GV. Experimental Investigation of Reykjavik City Footbridge. In: The 28th International Modal Analysis Conference. Jacksonville, Florida, USA. 1–4 February, 2010.
[67] Gudmundsson GV, Ingólfsson ET, Einarsson B, Bessason B. Serviceability assessment of three lively footbridges in Reykjavik. In: The 3rd International Conference Footbridge. Porto, Portugal. 2–4 July, 2008.
[68] Brownjohn JMW, Bocian M, Hester D, Quattrone A, Hudson W, Moore D, et al. Footbridge system identification using wireless inertial measurement units for force and response measurements. J Sound Vib 2016;384:339–55.
[69] Zuo D, Hua J, Van Landuyt D. A model of pedestrian-induced bridge vibration based on full-scale measurement. Eng Struct 2012;45:117–26.
[70] Vladimír Š, Michal P, Tomáš P. A dynamic analysis of the cable-stayed footbridge in Čelákovice Town. Procedia Eng 2017;199:2877–82.
[71] Butz C, Feldmann M, Heinemeyer C, Sedlacek G, Chabrolin B, Lemaire A, et al. Advanced load models for synchronous pedestrian excitation and optimised design guidelines for steel footbridges (SYNPEX). RFCS-Research Project RFS-CR-03019; 2007.
[72] Eutinger Waagsteg Bridge. https://structurae.net/structures/eutinger-waagsteg [accessed 04 December 2018].
[73] Katzbuckelbruecke Footbridge. https://structurae.net/structures/innenhafen-footbridge [accessed 04 December 2018].
[74] Bayraktar A, Altunişik Ahmet C, Sevim B, Türker T. Modal testing, finite-element model updating, and dynamic analysis of an arch type steel footbridge. J Perform Constr Facil 2009;23:81–9.
[75] Caetano E, Cunha A, Moutinho C. Implementation of passive devices for vibration control at Coimbra footbridge. In: The 2nd International Conference on Experimental Vibration Analysis for Civil Engineering Structures. Porto, Portugal. October, 2007.
[76] Breman C, Stuit H, Snijder H. Dynamic analysis of the Rotterdam Central Station Footbridge. In: The 4th International Footbridge Conference. Wroclaw, Poland. 6-8 July, 2011.
[77] Bassoli E, Gambarelli P, Simonini L, Vincenzi L. Dynamic analyses of a curved cable-

stayed footbridge under human induced vibrations: numerical models and experimental tests. In: The 5th ECCOMAS Thematic Conference on Computational Methods in Structural Dynamics and Earthquake Engineering. Crete Island, Greece. 25–27 May 2015.
[78] Kumar A. Investigation of the dynamic performance of a cable-stayed footbridge [PhD Thesis] University of Trento; 2011.
[79] Drygala IJ, Dulinska JM. A theoretical and experimental evaluation of the modal properties of a cable-stayed footbridge. Procedia Eng 2017;199:2937–42.
[80] Bernagozzi G, Landi L, Diotallevi PP. Modal testing through force vibrations of a timber footbridge. In: The 34th International Modal Analysis Conference. Orlando, Florida. 25–28 January, 2016.
[81] Rönnquist A, Strømmen E, Wollebæk L. Dynamic properties from full scale recordings and FE-modelling of a slender footbridge with flexible connections. Struct Eng Int 2008;18:421–6.
[82] Freedman G, Kermani A. Performance of a stress-laminated-timber arch bridge. Proc Inst Civ Eng Bridge Eng 2006;158:155–64.
[83] Poništová L, Fojtík R, Mareček D, Vašková V, Lokaj A. Response of wooden footbridge to the dynamic load. ARPN J Eng Appl Sci 2018;13:1943–50.
[84] BSI. NA to BS EN 1991-2:2003: UK National Annex to Eurocode 1: actions on structures – Part 2: traffic loads on bridges. London, UK: British Standards Institution; 2008.
[85] ISO. ISO 10137: 2007(E): bases for design of structures: serviceability of buildings and walkways against vibrations. Geneva: International Organization for Standardization; 2007.
[86] AASHTO. Guide specifications for design of FRP pedestrian bridges. first ed. Washington, DC: American Association of State Highway and Transportation Officials; 2008.
[87] Coleman TF, Li Y. An interior, trust region approach for nonlinear minimization subject to bounds. SIAM J Optim 1996;6:418–45.
[88] Bachmann H, Ammann WJ, Deischl F, Eisenmann J, Floegl I, Hirsch GH, et al. Vibration problems in structures: practical guidelines. Birkhäuser; 2012.
[89] AASHTO. LRFD bridge design specifications. Washington, DC: American Association of State Highway and Transportation Officials; 2012.
[90] CEN. EN 1995-2 Eurocode 5: design of timber structures – Part 2: bridges. Brussels: The European Committee for Standardisation; 2004.
[91] Glacisbruecke Footbridge. https://structurae.net/structures/glacis-footbridge [accessed 04 December 2018].
[92] Clough RW, Penzien J. Dynamics of structures. second ed. New York, NY, USA: McGraw-Hill; 1993.
[93] Erzbahnschwinge Footbridge. https://structurae.net/structures/erzbahnschwinge [accessed 04 December 2018].